Journal of Solid State Chemistry **146,** 176–183 (1999)
Article ID jssc.1999.8327, available online at http://www.idealibrary.com on IDEAL®

Perovskite-Type Oxides

II. Redox Properties of $LaMn_{1-x}Cu_xO_3$ and $LaCo_{1-x}Cu_xO_3$ and Methane Catalytic Combustion

Luciana Lisi,*,[1] Giovanni Bagnasco,† Paolo Ciambelli,‡ Sergio De Rossi,§ Piero Porta,§ Gennaro Russo,† and Maria Turco†

*Istituto di Ricerche sulla Combustione, c/o Dipartimento di Ingegneria Chimica, CNR, Piazzale V. Tecchio 80, 80125 Naples, Italy; †Dipartimento di Ingegneria Chimica, Università "Federico II," Naples, Italy; ‡Dipartimento di Ingegneria Chimica e Alimentare, Università di Salerno, Salerno, Italy; and §Centro di Studio del CNR su "Struttura e Attività Catalitica di Sistemi di Ossidi" (SACSO), c/o Dipartimento di Chimica, Università "La Sapienza," Piazzale A. Moro 5, 00185 Rome, Italy

Received October 22, 1998; in revised form March 22, 1999; accepted April 12, 1999

Redox properties of high-surface-area $LaM_{1-x}Cu_xO_3$ (M = Mn or Co) perovskites prepared by the citrate method were studied by H_2 TPR and O_2 TPD techniques. We have found that the reduction of Mn^{4+} occurs in all La–Mn–Cu perovskites at temperatures lower than that of Co^{3+} in La–Co–Cu samples. The presence of copper affects the reduction of both Mn^{4+} and Co^{3+}, increasing the temperature of reduction. Furthermore, Mn-based perovskites with a low Cu substitution ($x < 0.4$) release a great amount of O_2 at high temperature. Catalytic activity toward methane combustion was investigated under diluted conditions (0.4% CH_4 and 10% O_2, N_2 as balance) in the temperature range 673–1073 K using a fixed bed reactor with a space velocity of 40,000 $N\,cm^3\,h^{-1}\,g^{-1}$. All samples catalyze methane oxidation in the temperature range 673–773 K, giving complete methane conversion below 1073 K and producing 100% CO_2. No deactivation phenomena were observed. Substitution with copper decreases catalytic activity. The higher activity of Mn-based perovskites compared with that of the corresponding Co samples with the same composition was attributed to the stronger oxidative properties of $LaM_{1-x}Cu_xO_3$. An apparent activation energy of 23 kcal mol^{-1} was evaluated on the basis of a first-order kinetic equation for all samples.

INTRODUCTION

Catalytic combustion has been proposed as a method for reducing thermal NO_x emissions due to the possibility of carrying out the reaction over a wider range of fuel/air ratios and at lower temperature compared with conventional flame combustion (1, 2). However, high-temperature applications, such as gas turbines, require materials stable to severe operating conditions (2, 3). Although noble metal-based catalysts show a very high specific activity, their utilization in combustors is limited by the high volatility of pure metals and their oxides and by the tendency toward sintering at moderate temperature (1, 2, 4).

Much attention has been paid recently to perovskite-type oxides, of general formula ABO_3, as catalysts for total oxidation of hydrocarbons due to their high activity and thermal stability (1, 2, 5). Most metallic elements are stable in the perovskite structure provided that the values of the cationic radii fit well the sizes of the 12-coordinated A and 6-coordinated B sites, e.g., $r_A > 0.90$ Å and $r_B > 0.51$ Å. Moreover, the high stability of the perovskite structure allows partial substitution of either A or B cation (6). Perovskite oxides are generally synthesized by ceramic methods that require very high temperature and produce materials with surface area lower than 5 $m^2\,g^{-1}$ (6), limiting to some extent their application.

Lanthanum-based perovskites containing cobalt, manganese, or iron as the B cation show catalytic activity close to that of noble metals (6, 7). According to the kinetic model proposed for hydrocarbon activation, weakly-adsorbed oxygen is involved in the reaction at low temperature whereas lattice oxygen becomes reactive at high temperature (6).

The effect of the partial substitution of the A cation, generally a rare-earth metal, with elements having a valence state different from 3+ has been widely studied (2, 6, 8). The best results at low temperature were obtained with the $La_{0.6}Sr_{0.4}MnO_3$ perovskite (2, 8) due to the enhancement of adsorbed oxygen in the anionic vacancies created by the La substitution. The effect of the substitution of the B cation (9, 10) and the application of $AB_{1-x}B'_xO_3$ perovskites to the catalytic combustion has been much less investigated. It has been reported (9, 10) that the substitution of copper for manganese leads to some modifications of the oxidative nonstoichiometry of $LaMnO_{3+\delta}$ perovskite depending on the Mn fraction substituted.

[1] To whom correspondence should be addressed. Fax: 39 081 5936936. E-mail: lisi@irc.na.cnr.it.

0022-4596/99 $30.00

In Part I the solid-state chemistry of the perovskite-type $LaMn_{1-x}Cu_xO_3$ and $LaCo_{1-x}Cu_xO_3$ solid solutions was described in detail (11). This paper reports on the redox properties and catalytic activity toward methane combustion. To our knowledge, this reaction has never been investigated in $LaM_{1-x}Cu_xO_3$ systems with M = Mn or Co.

EXPERIMENTAL

Catalyst Preparation and Physicochemical Characterization

Perovskite samples of general formula $LaM_{1-x}Cu_xO_3$ (M = Mn or Co and $x = 0, 0.2, 0.4, 0.6, 0.8, 1$) were prepared by metal citrate decomposition and calcined at 1073 K for 5 h. Table 1 reports the real compositions of all the samples studied, whereas in the following, for the sake of brevity, the materials are indicated by nondefective formulas. The details of the catalyst preparation and their physicochemical characterization (structural, magnetic, and morphological properties) are reported in Part I (11).

Redox Properties and Catalytic Activity Tests

Temperature programmed desorption (TPD) of O_2 and temperature-programmed reduction (TPR) with H_2 were performed using a Micromeritics TPD/TPR 2900 analyzer equipped with a TCD and coupled with a Hiden HPR 20 mass spectrometer. The sample (30 mg) was preheated in flowing air at 1073 K for 2 h before each TPD or TPR test. In TPR analyses a 2% H_2/Ar mixture (25 $cm^3\,min^{-1}$) was used to reduce the sample by heating 10 $K\,min^{-1}$ up to 1073 K. Water produced by the sample reduction was condensed in a cold trap before reaching the detectors. In O_2 TPD analyses the sample was heated 10 $K\,min^{-1}$ up to 1073 K in flowing He (25 $cm^3\,min^{-1}$).

Catalytic activity tests were carried out in a flow apparatus equipped with a fixed bed reactor in the temperature range 673–1073 K at atmospheric pressure. The molar feed composition was 0.4% CH_4, 10% O_2, balance N_2. The catalyst (particle size 180–250 μm), diluted 1 : 10 with quartz powder to limit thermal effects, was placed on a porous septum. Moreover, the narrowing of the reactor diameter in both the pre- and the postcatalytic zone and the presence of γ-Al_2O_3 pellets upside the catalytic bed limited the occurrence of homogeneous reactions. The temperature was monitored with a type K thermocouple located in the catalyst bed.

The space velocity was 40,000 $N\,cm^3\,h^{-1}\,g^{-1}$ in all catalytic tests. CH_4, CO, CO_2, and C_2 hydrocarbon analysis was effected with a Hewlett–Packard 6890 gas chromatograph with Poraplot Q and 5A Molecular Sieve capillary columns. Carbon balance was closed to within $\pm 5\%$ in all catalytic tests.

TABLE 1
Crystalline Phase, Surface Area, and Catalyst Composition

Catalyst	Crystalline phase[a]	Surface area ($m^2\,g^{-1}$)	Composition
$LaMn_{1-x}Cu_xO_3$			
$x = 0$	P	22	$La_{0.95}Mn^{3+}_{0.62}Mn^{4+}_{0.33}O_3$
$x = 0.2$	P	19	$La_{0.95}Mn^{3+}_{0.33}Mn^{4+}_{0.44}Cu_{0.19}O_3$
$x = 0.4$	P	14	$LaMn^{3+}_{0.19}Mn^{4+}_{0.41}Cu_{0.40}O_3$
$x = 0.6$	P	20	$LaMn^{4+}_{0.40}Cu_{0.60}O_{2.9}$
$x = 0.8$	P, T, La_2CuO_4	15	
$LaCo_{1-x}Cu_xO_3$			
$x = 0$	P	15	$LaCoO_3$
$x = 0.2$	P	21	$LaCo_{0.80}Cu_{0.20}O_{2.9}$
$x = 0.4$	P, La_2CuO_4	13	$LaCo_{0.60}Cu_{0.40}O_{2.8}$
$x = 0.6$	P, T, La_2CuO_4	19	
$x = 0.8$	P, T, La_2CuO_4	15	
$x = 1$	T, La_2CuO_4	<1	

[a] P, perovskite; T, tenorite.

RESULTS AND DISCUSSION

Physicochemical Characterization

In Table 1 the main features of the perovskite samples in terms of phases present, surface area, and chemical composition are reported. Their structural, magnetic, and morphological properties were described in Part I (11).

The main results of solid-state chemistry characterization of the materials are summarized here to better correlate with their redox and catalytic properties:

i. $LaM_{1-x}Cu_xO_3$ samples prepared at 1073 K are perovskite-like single phases up to $x = 0.6$ for M = Mn and $x = 0.2$ for M = Co. CuO and La_2CuO_4 phases are present in addition to the perovskite at higher Cu contents up to $x = 1$, when they are the only phases present due to the instability of the $LaCuO_3$ structure under these experimental conditions (10). The results concerning the Mn-based samples are in agreement with those obtained by Rojas *et al.* (10), who found the same upper limit for the stability of the perovskite structure and the formation of CuO and La_2CuO_4 for $x > 0.6$ for $LaMn_{1-x}Cu_xO_3$ samples.

ii. No Co^{4+} is present in the $LaCo_{1-x}Cu_xO_3$ samples. In this system the lower Cu^{2+} charge is balanced by oxygen vacancies, whose amount increases with the increase in copper content.

iii. Mn^{4+} was detected in all Mn-based samples. The $LaMnO_3$ nonsubstituted sample itself contains a substantial fraction of Mn^{4+} (35%) which increases with copper substitution up to $x = 0.6$ when it reaches 100%. For $x = 0.2$ and $x = 0.4$ the charge defectivity due to Cu^{2+} incorporation is balanced by Mn^{3+} oxidation to Mn^{4+}. $LaMnO_3$ and

$LaMn_{0.8}Cu_{0.2}O_3$ contain small equal amounts ($\cong 0.05$) of *A* and *B* cation vacancies, $LaMn_{0.6}Cu_{0.4}O_3$ is a nondefective perovskite, while in $LaMn_{0.4}Cu_{0.6}O_3$ a loss of oxygen (3.3%) compensates the additional copper incorporation (see Table 1).

iv. Specific surface areas are about 15–20 $m^2 g^{-1}$ for all samples except for that with $x = 1$ (CuO + La_2CuO_4) whose value was $< 1\ m^2 g^{-1}$.

Redox Properties

Only O_2 was detected in the outlet gas of TPD measurements. O_2 TPD spectra (nor reported) show two peaks for all catalysts, the former with the maximum in the temperature range 513–733 K and the latter with the maximum in the range 913–1073 K. The amount of oxygen related to the low-temperature peak is very small for all catalysts while that evolved at high temperature ranges from 0.024 to 0.20 mol O_2 (total moles of transition metal cation)$^{-1}$, the maximum value being given by $LaMnO_3$. The first peak, referred to as the α peak, was attributed to oxygen species weakly bound to the surface while the second peak (β peak) was related to the reduction of *B* cations to lower oxidation state (7) in the ABO_3 structure. The values of O_2 released at both low and high temperature suggest that the oxygen evolution must be related only to the catalyst surface since larger amounts of O_2 should be expected for a phenomenon involving the bulk of the sample. Consequently, in Table 2 the amount of oxygen released by the catalysts is referred to the surface area. XRPD analysis performed on the samples after the TPD experiments indicates that no phase transformation occurred, confirming the previous hypothesis.

Concerning the Mn-based perovskites, $LaMnO_3$ and $LaMn_{0.8}Cu_{0.2}O_3$ give rise to a strong signal at high temperature, which is markedly decreased by additional copper substitution. These results suggest that the high values of the β peak, associated with the reduction of the *B* cation, are obtained when cationic vacancies are present ($x < 0.4$).

TABLE 2
O_2 Evolution in TPD Experiments

	O_2 evolution $\times 10^6$ (mol m^{-2})		
Catalyst	Total	Low *T* (α peak)	High *T* (β peak)
$LaMn_{1-x}Cu_xO_3$			
$x = 0$	2.25	0.08	2.17
$x = 0.2$	2.16	0.01	2.15
$x = 0.4$	0.12	0.03	0.09
$LaCo_{1-x}Cu_xO_3$			
$x = 0$	0.29	0.15	0.14
$x = 0.2$	1.38	0.32	1.06
$x = 1$	0.34	0.14	0.20

With respect to the Co-based perovskite samples, the amounts of O_2 released at low and high temperature are low and comparable for $LaCoO_3$, whereas both α and, especially, β peaks increase for the sample $LaCo_{0.8}Cu_{0.2}O_3$ (see Table 2). Amounts of O_2 comparable to those found by us for the two nonsubstituted Mn- and Co-based perovskites were found by Nitadori *et al.* (12) for $LaMnO_3$ and by Nitadori and Misono (13) for $LaCoO_3$ below 773 K. For $LaCoO_3$, however, a conspicuous evolution of oxygen starting at $T > 773$ K is reported (13) in contrast to the present results.

The reversibility of the O_2 release process was verified by performing a second TPD experiment after further treatment of the sample for 2 h in flowing air at 1073 K. The complete superimposition of the first and the second TPD profiles for all catalysts confirms the reversibility of the process. XRPD spectra performed after O_2 TPD cycles accordingly showed that the structure of catalysts was unchanged.

In TPR measurements only H_2 was detected in the outlet gas, confirming the effectiveness of the cold trap. TPR curves, reported in Fig. 1, show two or more peaks for all catalysts, suggesting the occurrence of a multiple-step reduction. For $LaMn_{1-x}Cu_xO_3$ perovskites the first signal is quite complex, with a maximum ranging from 573 to 673 K, while the second step of the reduction, starting just before 1073 K, refers to constant temperature.

The first signal in the TPR profile of the nonsubstituted $LaMnO_3$ perovskite has the maximum at 673 K and a shoulder at higher temperature. The peak temperature of this signal shifts to 573 K for the $LaMn_{0.8}Cu_{0.2}O_3$ sample with the shoulder still present in the range 673–773 K. By increasing the manganese substitution up to $x = 0.4$ the maximum of the first peak further decreases ($T_{max} = 508$ K) and the shoulder is detectable as a distinct peak with a maximum at about 673 K. For the $LaMn_{0.4}Cu_{0.6}O_3$ sample, however, a single peak with the maximum at 623 K appears. In all TPR experiments of Mn-based samples the baseline was not recovered after the first peak, indicating that the reduction associated with the first peak is still occurring when the successive step of the reduction starts.

In the TPR profile of the $LaCoO_3$ perovskite three peaks are detectable: the first one with the maximum at 753 K, and the second and third peaks, substantially overlapping, with maxima at 923 and 1028 K, respectively. For the $LaCo_{0.8}Cu_{0.2}O_3$ sample only two signals appear with maxima at 623 and 853 K. Finally, the sample with $x = 1$ shows a signal, likely composed of two peaks, with a maximum at 608 K and a very small peak with a maximum at 708 K.

In Table 3 for all catalysts the total H_2 uptake and the fractions measured in the low- and high-temperature regions are compared with the amounts calculated from the associated reactions (also shown in Table 3) and the catalyst composition. For the $LaCoO_3$ perovskite the amount of H_2

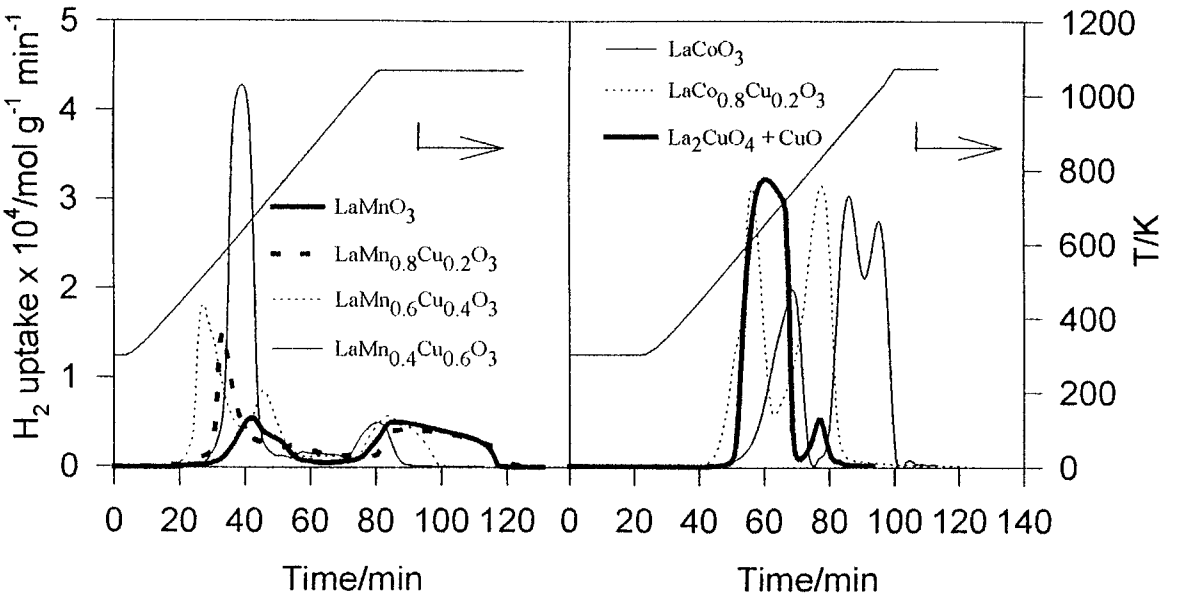

FIG. 1. TPR profiles of $LaM_{1-x}Cu_xO_3$ samples.

consumed provides evidence of the complete reduction of Co^{3+} to Co^0 occurring in two steps, from Co^{3+} to Co^{2+} and from Co^{2+} to Co^0, in agreement with the results of Baiker *et al.* (14) and Futai *et al.* (15). For the $LaCo_{0.8}Cu_{0.2}O_3$ sample the same double-step reduction of cobalt can be assumed. In this case, however, the total reduction of Cu^{2+} to Cu^0 is expected to contribute to the H_2 consumption corresponding to the first signal. The XRD analysis carried out on Co-based perovskites after the TPR experiments evidenced the formation of La_2O_3 and/or $La(OH)_3$ (coming from the hydration of La_2O_3), metallic Co, and metallic Cu, when present in the sample composition, in agreement with the TPR results.

The total reduction of copper from Cu^{2+} to Cu^0 can be supposed to occur also in the mixed sample with $x = 1$ according to both the H_2 uptake and the results of the XRPD analysis. Nevertheless, the large superimposition of the signals does not allow the determination of the sequence of copper reduction in CuO and La_2CuO_4. Under different conditions Rojas *et al.* (10) detected two reduction steps for the same sample, attributing the reduction occurring at lower temperature to CuO and that occurring at higher temperature to the more stable La_2CuO_4.

The reduction of Mn-based perovskites is much more complex due to the simultaneous presence of Mn^{3+} and Mn^{4+} in the starting material. The XRD analysis, performed after the TPR experiment, shows the presence of La_2O_3 and/or $La(OH)_3$, MnO, and metallic Cu, indicating that copper undergoes a complete reduction, whereas Mn^{4+} and Mn^{3+} are reduced to only the 2+ oxidation state, as also observed by Rojas *et al.* (10). The values for H_2 uptake reported in Table 3 suggest that the first peak can be related both to the reduction of Cu^{2+} to Cu^0, when copper is present, and to the reduction of Mn^{4+} to Mn^{3+}, whereas the second peak can be attributed to the reduction of Mn^{3+} to Mn^{2+}, being quite proportional to the total manganese content. Rojas *et al.* (10) found two reduction steps for $LaMn_{1-x}Cu_xO_3$ perovskites, the first associated with the reduction of Cu^{2+} to Cu^0 and the second associated with the reduction of Mn^{n+} to Mn^{2+}. The two steps were not well separated, thus indicating that the reduction of manganese starts before the reduction of Cu^{2+} is completed. The data reported in the present paper, however, seem to suggest that the reduction of copper contained in the perovskite structure takes place before the reduction of Mn^{4+} to Mn^{3+}. A rough separation of the two partially overlapped peaks in the low temperature range of the TPR curve of the $LaMn_{0.6}Cu_{0.4}O_3$ perovskite showed that the area of the signal with the maximum at 508 K corresponds well to the H_2 consumed for the reduction of copper contained in this sample from Cu^{2+} to Cu^0. As a consequence, the reduction of copper from Cu^{2+} to Cu^0 should start before the reduction of manganese from Mn^{4+} to Mn^{3+}. Furthermore, the first step in the reduction of manganese occurs at higher temperature compared with that associated with the $LaMnO_3$ perovskite. Although a separation of the first two peaks cannot be attempted for the other systems, the same trend can be supposed for the other Mn-based perovskites. Therefore, the presence of copper in the perovskite structure seems to stabilize Mn^{4+} toward the reduction since in substituted samples the reduction to Mn^{3+} occurs at slightly higher temperature compared with $LaMnO_3$ perovskite.

TABLE 3
H_2 Uptake in TPR Experiments, Starting Temperature of Reduction, T_{onset}, and Associated Reactions

Catalyst	T_{onset} (K)		H_2 uptake (mol H_2 mol^{-1} M[a]) Exp.	Calc.[b]	Associated reactions
$LaMn_{1-x}Cu_xO_3$					
$x = 0$	427	Total	0.59	0.65	
		Low temperature	0.21	0.17	$Mn^{4+} + e^- \rightarrow Mn^{3+}$
		High temperature	0.38	0.48	$Mn^{3+} + e^- \rightarrow Mn^{2+}$
$x = 0.2$	419	Total	0.72	0.79	
		Low temperature	0.39	0.41	$Mn^{4+} + e^- \rightarrow Mn^{3+}$ $Cu^{2+} + 2e^- \rightarrow Cu^0$
		High temperature	0.33	0.38	$Mn^{3+} + e^- \rightarrow Mn^{2+}$
$x = 0.4$	414	Total	0.87	0.90	
		Low temperature	0.62	0.61	$Mn^{4+} + e^- \rightarrow Mn^{3+}$ $Cu^{2+} + 2e^- \rightarrow Cu^0$
		High temperature	0.25	0.29	$Mn^{3+} + e^- \rightarrow Mn^{2+}$
$x = 0.6$	416	Total	1.08	1.00	
		Low temperature	0.92	0.80	$Mn^{4+} + e^- \rightarrow Mn^{3+}$ $Cu^{2+} + 2e^- \rightarrow Cu^0$
		High temperature	0.16	0.20	$Mn^{3+} + e^- \rightarrow Mn^{2+}$
$LaCo_{1-x}Cu_xO_3$					
$x = 0$	467	Total	1.54	1.50	
		Low temperature	0.48	0.50	$Co^{3+} + e^- \rightarrow Co^{2+}$
		High temperature	1.06	1.00	$Co^{2+} + 2e^- \rightarrow Co^0$
$x = 0.2$	460	Total	1.47	1.40	
		Low temperature	0.67	0.60	$Co^{3+} + e^- \rightarrow Co^{2+}$ $Cu^{2+} + 2e^- \rightarrow Cu^0$
		High temperature	0.80	0.80	$Co^{2+} + 2e^- \rightarrow Co^0$
$x = 1$	469	Total	1.08	1.00	$Cu^{2+} + 2e^- \rightarrow Cu^0$

[a] M in substituted samples refers to the total amount of transition metal cations.
[b] Calculated according to the occurring reactions (last column) and stoichiometric compositions shown in Table 1.

In summary, a comparison of the experimental and theoretical values of H_2 uptake in Table 3 supports, within experimental error, the following view: (i) in the low-temperature TPR region the reductions of Mn^{4+} to Mn^{3+} and Cu^{2+} to Cu^0 occur for $LaMn_{1-x}Cu_xO_3$ systems, whereas for $LaCo_{1-x}Cu_xO_3$ systems the reductions of Co^{3+} to Co^{2+} and Cu^{2+} to Cu^0 take place; (ii) in the high-temperature region reduction of Mn^{3+} to Mn^{2+} occurs for the former system, whereas reduction of Co^{2+} to Co^0 occurs for the latter.

The results (not shown) of an XRD analysis of the phases present in the samples coming from TPR experiments interrupted at the end of the low-temperature reduction region were found to be fully consistent with the above reduction sequence.

In particular we found that the evolution of the samples after the first TPR peak, as monitored by XRD, depended on their composition. Specifically, for $x = 0$ and 0.2 the perovskite structure was preserved. For $x = 0.4$ the perovskite coexisted with La_2O_3, $La(OH)_3$, and metal copper. For $x = 0.6$ the perovskite structure was completely destroyed and only the lines of La_2O_3, $La(OH)_3$ and metal copper were present in the spectrum. Mn_2O_3 expected on the basis of the hypothesized reduction sequence was not detected probably because it was in a finely dispersed status.

Some samples after TPR in hydrogen up to 1073 K were submitted to reoxidation in air at 1073 K and a second TPR was carried out. The two TPR profiles were very close, indicating that the reduction process was reversible. To check this point, XRD spectra of samples reoxidized in air at 1073 K after H_2 TPR were recorded. Surprisingly, the analysis showed that the perovskite phase was restored on reoxidizing treatment. As an example, Fig. 2 shows the case of $La_{0.95}Mn_{0.76}Cu_{0.19}O_3$. It appears that after the reoxidation treatment a perovskite phase is restored, but with higher symmetry compared with the starting material. The effective mixing of the particles of the various phases present in reduced samples is suggested to be the reason for the ease

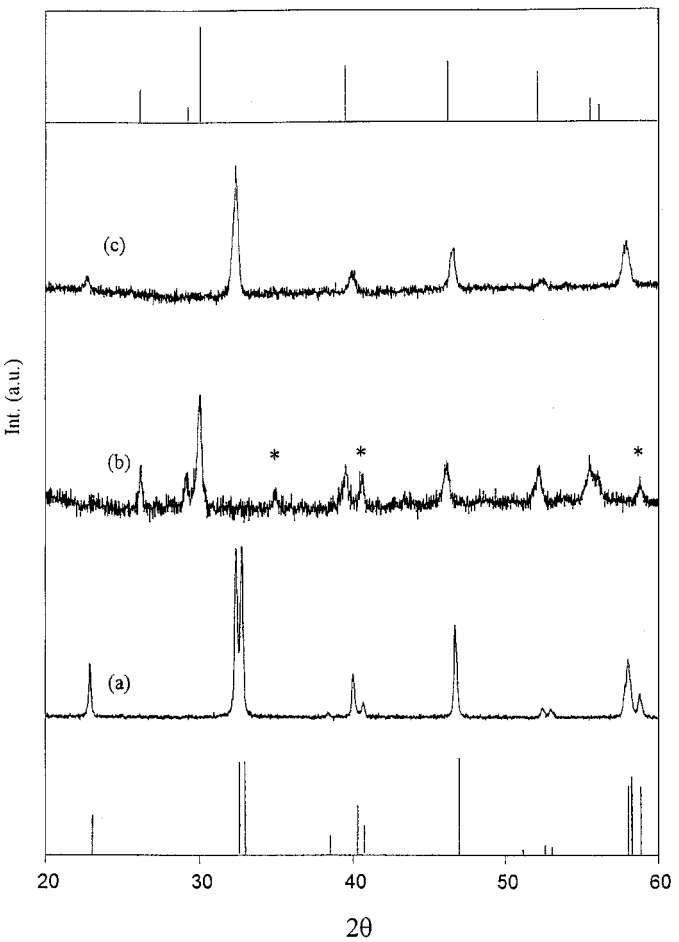

FIG. 2. Powder X-ray diffraction patterns for (a) $La_{0.95}Mn_{0.76}Cu_{0.19}O_3$ calcined in air at 1073 K, (b) after TPR experiment up to 1073 K, and (c) after reoxidation in air at 1073 K 0.5 h. XRD lines of $LaMnO_{3.15}$ (ASTM Card 32-484) and La_2O_3 (ASTM Card 36-1481) are reported at the bottom and the top, respectively. The peaks labeled with asterisks belong to MnO (ASTM Card 4-326).

of reconstruction of the perovskite structure occurring at relatively mild conditions.

Catalytic Activity

Preliminary tests of methane combustion, carried out in the absence of the catalyst, showed no methane conversion up to 1023 K. At 1073 K 8% methane conversion was observed, producing CO (80%) and CO_2 (20%).

Some results of catalytic activity measurements are reported in Fig. 3. In the presence of the catalyst the reaction starts in the range 673–773 K, depending on the activity of the sample. Complete oxidation of methane occurs below 1073 K, only CO_2 having been detected in the outlet gas for all catalytic tests. $LaMnO_3$ perovskite is the most active catalyst, giving 10% CH_4 conversion at 673 K and reaching 50% conversion at 773 K. A temperature of 923 K is sufficient to obtain 100% conversion. On the other hand, $LaCoO_3$ perovskite gives 10% CH_4 conversion at 723 K, 50% conversion at 853 K, and total conversion at 1033 K. In general, Mn-based perovskites are more active than the corresponding Co-based samples with the same Cu content and the copper substitution results in decreasing the catalyst performance of both $LaMnO_3$ and $LaCoO_3$ perovskites up to $x = 1$. The mixed sample composed of CuO and La_2CuO_4 shows the lowest activity. Nevertheless, total methane conversion is reached at 1073 K despite the very low surface area of this sample.

After the first cycle of activity tests the catalyst was cooled down and a second cycle of measurements carried out. The reproducibility of the results provides evidence of the stability of phases and the absence of deactivation phenomena.

Two different reaction mechanisms have been proposed for perovskite oxides involving two different oxygen species (6, 16). At low temperature an Eley–Rideal mechanism occurring between adsorbed oxygen and gaseous CH_4 has been assumed. At high temperature, when the coverage of molecular O_2 strongly decreases, lattice oxygen becomes active and the methane oxidation can be described by a redox mechanism. In this case, lattice reoxidation is very fast and a zero-order dependence on oxygen partial pressure is expected.

The catalytic activity data were elaborated on the basis of the first-order kinetic equation $r = kpCH_4$, taking into account the large O_2 excess, and Arrhenius plots were drawn for all catalysts (Fig. 4). The good linear correlation obtained for all samples suggests that in the range of operational conditions investigated the kinetics is not influenced by diffusion limitations.

The apparent activation energy was about the same (23 kcal mol^{-1}) for all samples. Similar values have been reported for $LaMnO_3$ (17), for $LaCoO_3$ perovskites (14, 17), and for $LaCuO_3$ (17).

In Table 4 the values of the preexponential factor, estimated from the Arrhenius plots, are reported. The Mn-based perovskites show higher values of the preexponential factors referred both to the catalyst weight and to the catalyst surface. The sample composed of CuO and La_2CuO_4 shows the lowest value of the preexponential factor referred to the catalyst weight as could be expected by its low catalytic activity. However, if the very small value of the surface area is considered, this sample shows the highest specific activity.

In conclusion, the preliminary kinetic analysis indicates that the data are well interpolated by a first-order rate equation suggesting that, in the whole range of conditions investigated, a reaction mechanism involving the lattice oxygen is likely operating on all catalysts. This was further confirmed by the better catalytic performance of the Mn-based perovskites which were found to have stronger

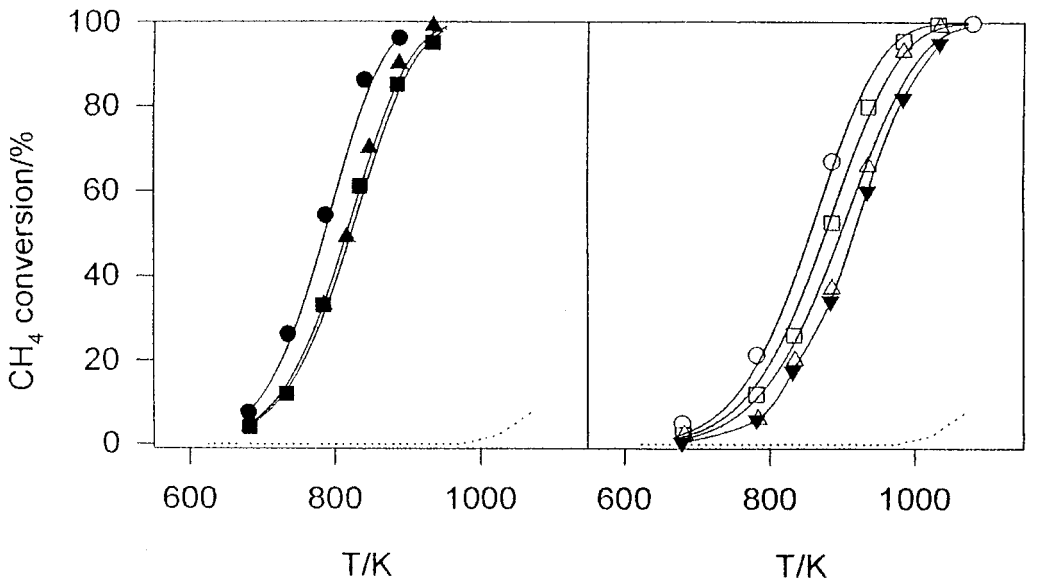

FIG. 3. Methane conversion as a function of the temperature for $LaM_{1-x}Cu_xO_3$ samples: $LaMnO_3$, ●; $LaMn_{0.8}Cu_{0.2}O_3$, ■; $LaMn_{0.6}Cu_{0.4}O_3$, ▲; $LaCoO_3$, ○; $LaCo_{0.8}Cu_{0.2}O_3$, □; $LaCo_{0.6}Cu_{0.4}O_3$, △; $La_2CuO_4 + CuO$, ▼. The dotted line represents conversion in the absence of catalyst.

oxidation properties compared with Co-based samples. In fact, the presence of weakly bound oxygen related to the anionic vacancies, observed mainly for Co-based perovskites, does not lead to enhancement of the catalytic activity. On the contrary, the easy reducibility of the Mn^{4+} ion, observed by both TPR and O_2 TPD analysis, gives rise to more active catalysts. Therefore, the substitution of Mn or Co cations with Cu, leading to an increase in oxygen vacancies in all $LaCo_{1-x}Cu_xO_3$ samples and in $LaMn_{1-x}Cu_xO_3$ samples with $x > 0.4$, does not result in an increase in catalytic activity in the range of experimental conditions reported in this paper. However, the results showed that the easy reducibility of the transition metal cation represents a good feature for a catalytic system operating under these

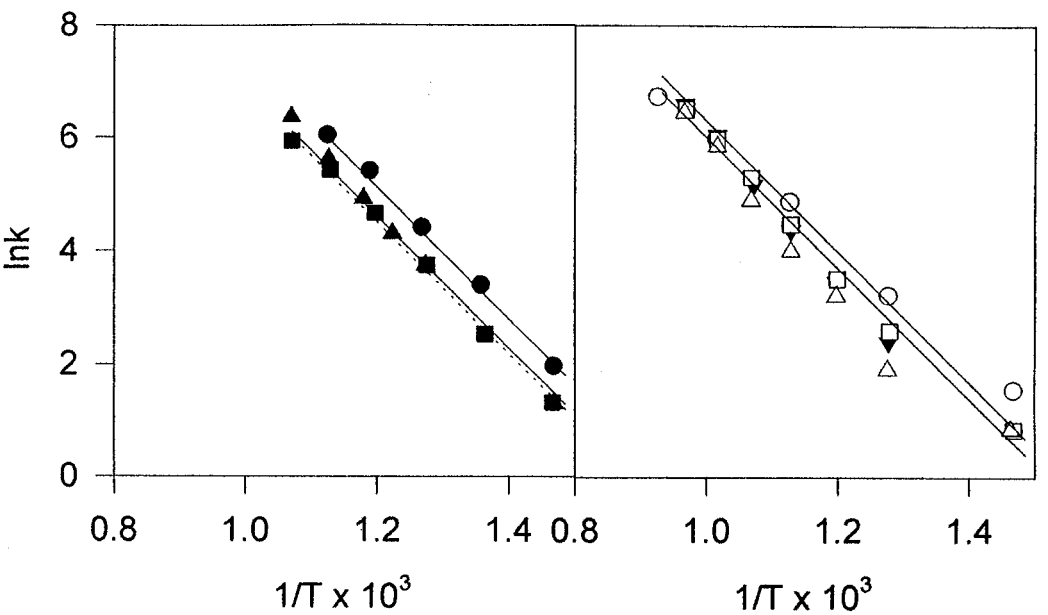

FIG. 4. Arrhenius plots for $LaM_{1-x}Cu_xO_3$ samples: $LaMnO_3$, ●; $LaMn_{0.8}Cu_{0.2}O_3$, ■; $LaMn_{0.6}Cu_{0.4}O_3$, ▲; $LaCoO_3$, ○; $LaCo_{0.8}Cu_{0.2}O_3$, □; $LaCo_{0.6}Cu_{0.4}O_3$, △; $La_2CuO_4 + CuO$, ▼.

TABLE 4
Preexponential Factors Referred to the Catalyst Weight (A_w) and to the Catalyst Surface (A_s)

Catalyst	$A_w \times 10^{-8}$ ($L\,h^{-1}\,g^{-1}$)	$A_s \times 10^{-6}$ ($L\,h^{-1}\,m^{-2}$)
$LaMn_{1-x}Cu_xO_3$		
$x = 0$	1.8	8.1
$x = 0.2$	1.0	5.3
$x = 0.4$	1.1	7.7
$LaCo_{1-x}Cu_xO_3$		
$x = 0$	0.6	4.1
$x = 0.2$	0.4	2.1
$x = 1$	0.3	>30

experimental conditions. Furthermore, the decrease in the value of the preexponential factors with increasing Cu substitution seems to suggest that the role of active sites is played by manganese and cobalt even though, when copper is the only transition metal cation present in the sample composition, it can act as an active site as well.

Concerning the manganese ions, it is quite difficult to determine whether Mn^{4+} or Mn^{3+} is involved in the catalytic reaction. In fact the activity only slightly decreases when passing from $LaMnO_3$, which has the higher fraction of Mn^{3+}, to the sample with $x = 0.4$, which has the higher fraction of Mn^{4+}, among the catalysts examined in catalysis. We suggest that the presence of the redox couple Mn^{4+}/Mn^{3+}, promoting the mobility of the lattice oxygen, is an important factor in determining the catalytic activity of the $LaMn_{1-x}Cu_xO_3$ system.

CONCLUSIONS

Mn^{4+} is more easily reducible than Co^{3+} as shown by the low temperature of reduction observed in TPR experiments. However, cobalt undergoes complete reduction from Co^{3+} to Co^0 whereas manganese is reduced only to Mn^{2+}. Copper is reduced from Cu^{2+} to Cu^0 and decreases the reducibility of the other transition metal cation present in the catalyst composition.

All samples catalyze the combustion of methane in the temperature range 573–1073 K leading to total oxidation to CO_2. Mn-based perovskites were found more active than the corresponding Co samples with the same composition. The copper substitution results in a slight decrease in catalytic activity. On all perovskites the same reaction mechanism involving lattice oxygen is operating. An apparent activation energy of 23 $kcal\,mol^{-1}$ was evaluated on the basis of a first-order rate equation. The best catalytic performance of $LaMn_{1-x}Cu_xO_3$ perovskites is attributed to the higher oxygen mobility shown by these samples.

REFERENCES

1. M. F. Zwinkels, S. G. Järås, and P. G. Menon, *Catal. Rev. Sci. Eng.* **35**(3), 319 (1993).
2. H. Arai and M. Machida, *Catal. Today* **10,** 81 (1991).
3. K. Eguchi and H. Arai, *Catal. Today* **29,** 379 (1996).
4. R. Burch, *Catal. Today* **35,** 27 (1997).
5. J. G. Mc Carty and H. Wise, *Catal. Today* **8,** 231 (1990).
6. L. G. Tejuca, J. L. G. Fierro, and J. M. D. Tascón, *Adv. Catal.* **36,** 237 (1989).
7. T. Seiyama, *Catal. Rev. Sci. Eng.* **34,** 281 (1992).
8. L. Marchetti and L. Forni, *Appl. Catal. B Environ.* **15,** 179 (1998).
9. E. M. Vogel, D. W. Johnson, Jr., and P. K. Gallagher, *J. Am. Ceram. Soc.* **60,** 31 (1977).
10. M. L. Rojas, J. L. G. Fierro, L. G. Tejuca, and A. T. Bell, *J. Catal.* **124,** 41 (1990).
11. P. Porta, S. De Rossi, M. Faticanti, G. Minelli, I. Pettiti, L. Lisi, and M. Turco, *J. Solid State Chem.* **145,** (1999).
12. T. Nitadori, S. Kurihara, and M. Misono, *J. Catal.* **98,** 221 (1985).
13. T. Nitadori and M. Misono, *J. Catal.* **93,** 459 (1985).
14. A. Baiker, P. E. Marti, P. Keusch, E. Fritsch, and A. Reller, *J. Catal.* **146,** 268 (1994).
15. M. Futai, C. Yonghua, and Louhui, *React. Kinet. Catal. Lett.* **31,** 47 (1986).
16. Z. Chen, T. Ling, and M. Lee, *React. Kinet. Catal. Lett.* **62,** 186 (1997).
17. H. Arai, T. Yamada, K. Eguchi, and T. Seiyama, *Appl. Catal.* **26,** 265 (1986).